Mon. Not. R. Astron. Soc. **354,** 1223–1238 (2004) doi:10.1111/j.1365-2966.2004.08282.x

Spectroscopic survey of the Galaxy with *Gaia* – I. Design and performance of the Radial Velocity Spectrometer

D. Katz,[1⋆] U. Munari,[2] M. Cropper,[3] T. Zwitter,[4] F. Thévenin,[5] M. David,[6] Y. Viala,[1] F. Crifo,[1] A. Gomboc,[7,4] F. Royer,[8,1] F. Arenou,[1] P. Marrese,[2] R. Sordo,[2] M. Wilkinson,[9] A. Vallenari,[10] C. Turon,[1] A. Helmi,[11] G. Bono,[12] M. Perryman,[13] A. Gómez,[1] L. Tomasella,[2] F. Boschi,[2] D. Morin,[1] M. Haywood,[1] C. Soubiran,[14] F. Castelli,[15,16] A. Bijaoui,[5] G. Bertelli,[10] A. Prsa,[4] S. Mignot,[1] A. Sellier,[1] M.-O. Baylac,[1] Y. Lebreton,[1] U. Jauregi,[4] A. Siviero,[2] R. Bingham,[17,3] F. Chemla,[1] J. Coker,[3] T. Dibbens,[3] B. Hancock,[3] A. Holland,[18] D. Horville,[1] J.-M. Huet,[1] P. Laporte,[1] T. Melse,[1] F. Sayède,[1] T.-J. Stevenson,[18] P. Vola,[1] D. Walton[3] and B. Winter[3]

[1] *Observatoire de Paris, GEPI, 5 Place Jules Janssen, F-92195 Meudon, France*
[2] *Osservatorio Astronomico di Padova INAF, sede di Asiago, 36012 Asiago (VI), Italy*
[3] *Mullard Space Science Laboratory, University College London, Holmbury St Mary, Dorking, Surrey RH5 6NT*
[4] *Department of Physics, University of Ljubljana, Jadranska 19, 1000 Ljubljana, Slovenia*
[5] *O.C.A., BP 4229, F-06304 Nice Cedex 4, France*
[6] *University of Antwerp, Middelheimlaan 1, B-2020 Antwerpen, Belgium*
[7] *Astrophysics Research Institute, Liverpool John Moores University, Twelve Quays House, Egerton Wharf, Birkenhead CH41 1LD*
[8] *Observatoire de Genève, 51 chemin des Maillettes, CH-1290 Sauverny, Switzerland*
[9] *Institute of Astronomy, Madingley Road, Cambridge CB3 0HA*
[10] *INAF – Osservatorio Astronomico di Padova, Vicolo Osservatorio 5, 35122 Padova, Italy*
[11] *Kapteyn Astronomical Institute, PO Box 800, 9700 AV Groningen, the Netherlands*
[12] *INAF – Rome Astronomical Observatory, Via Frascati 33, 00040 Monte Porzio Catone, Italy*
[13] *Research and Scientific Support Department of ESA, ESTEC, Postbus 299, Keplerlaan 1, Noordwijk NL-2200 AG, the Netherlands*
[14] *Observatoire Aquitain des Sciences de l'Univers, UMR 5804, 2 rue de l'Observatoire, F-33270 Floirac, France*
[15] *CNR-Istituto di Astrofisica Spaziale e Fisica Cosmica, Via del Fosso del Cavaliere, 00133 Roma, Italy*
[16] *INAF – Osservatorio Astronomico di Trieste, via G.B. Tiepolo 11, 34131 Trieste, Italy*
[17] *Optical Design Service, Cambridge, 29 Millington Road, Cambridge CB3 9HW*
[18] *University of Leicester, Space Research Centre, University Road, Leicester LE1 7RH*

Accepted 2004 August 4. Received 2004 August 1; in original form 2004 June 9

ABSTRACT

The definition and optimization studies for the *Gaia* satellite spectrograph, the 'radial velocity spectrometer' (RVS), converged in late 2002 with the adoption of the instrument baseline. This paper reviews the characteristics of the selected configuration and presents its expected performance. The RVS is a 2.0 × 1.6 degree integral field spectrograph, dispersing the light of all sources entering its field of view with a resolving power $R = \lambda/\Delta\lambda = 11\,500$ over the wavelength range [848, 874] nm. The RVS will continuously and repeatedly scan the sky during the 5-yr *Gaia* mission. On average, each source will be observed 102 times over this period. The RVS will collect the spectra of about 100–150 million stars up to magnitude $V \simeq$ 17–18. At the end of the mission, the RVS will provide radial velocities with precisions of ∼2 km s^{-1} at $V = 15$ and ∼15–20 km s^{-1} at $V = 17$, for a solar-metallicity G5 dwarf. The RVS will also provide rotational velocities, with precisions (at the end of the mission) for late-type stars of $\sigma_{v \sin i} \simeq 5$ km s^{-1} at $V \simeq 15$ as well as atmospheric parameters up to $V \simeq$ 14–15. The individual abundances of elements such as silicon and magnesium, vital for the understanding of Galactic evolution, will be obtained up to $V \simeq$ 12–13. Finally, the presence of the 862.0-nm

⋆E-mail: david.katz@obspm.fr

diffuse interstellar band (DIB) in the RVS wavelength range will make it possible to derive the three-dimensional structure of the interstellar reddening.

Key words: instrumentation: spectrographs – space vehicles: instruments – techniques: radial velocities – techniques: spectroscopic.

1 INTRODUCTION

Understanding the Milky Way and its neighbourhood, both as a template for the formation and evolution of galaxies and as a stellar-physics laboratory, is one of the great astrophysics challenges at the beginning of the 21st century. The *Gaia* satellite (Perryman et al. 2001) was conceived and designed to constitute a major leap forward in this field. *Gaia* was selected as a Cornerstone of the European Space Agency (ESA) Horizon 2000+ programme in October 2000 and confirmed as part of the ESA Cosmic Vision programme in May 2002 and again in November 2003. The satellite launch is scheduled to take place 'no later than 2012' and all the current scientific and industrial studies are consistent with a launch date in mid-2010.

Gaia's payload consists of three instruments: an astrometric instrument, a multi-band photometer (observing in five broad- and 11 medium-band filters) and a spectrometer that will continuously and repeatedly scan the sky during the 5-yr mission. On average, 102 spectra will be obtained per source. The astro-photometric 'sample' will be complete up to the *Gaia* magnitude $G = 20$ ($G - V \simeq -0.36$ for a solar-metallicity G5 V star) and will contain more than a billion stars from the Galaxy and the Local Group. The huge size of the sample (about 1 per cent of the entire stellar content of the Milky Way galaxy) and the accuracy and wealth of information collected about the spatial, kinematic and chemical distributions of the stars will allow *Gaia* to decipher many aspects of the origin and evolution of our Galaxy. Moreover, given the very-large number of stars surveyed, even the briefest stages of stellar evolution have a very-high probability of being observed by *Gaia*. *Gaia* will also detect and characterize several thousand extra-solar planetary systems. It will observe some 10^5 to 10^6 minor bodies in the solar system, thousands of galaxies, some 5×10^5 quasars, about 10^5 extragalactic supernovae and will provide an accurate determination of several fundamental physical and cosmological parameters (e.g. γ, $\dot{G}/G$, Ω_M or Ω_Λ).

The initial concept of *Gaia* was developed around the astrometric instrument. However, based on the experience of *Hipparcos* (Gerbaldi et al. 1989; Mayor et al. 1989; Binney et al. 1997), it was clear that the capability of making radial velocity measurements would be central to the successful attainment of the main *Gaia* science goals. By supplying the third component of the velocity vector (the other two being provided by the tangential motions), the velocity along the line of sight is crucial for our understanding of the kinematics and dynamics of the Galaxy. Radial velocities are also necessary to correct the astrometric data for perspective acceleration (an apparent displacement on the sky induced by line-of-sight motion and which varies quadratically with time): simulations predict that the proper motions and positions of $\simeq 10^5$ stars (unknown a priori) would be significantly biased if this effect were not removed. Finally, multi-epoch radial velocities are extremely valuable for the detection and characterization of multiple systems and stellar variability. As *Gaia* was taking shape, several studies investigated the feasibility, merits and drawbacks of the acquisition of radial velocities from the ground and from space (Favata & Perryman 1995; Perryman 1995). In 1997, the decision was made to include a spectrograph on board *Gaia*.

A first concept of the spectrograph was designed in 1998 by Matra Marconi Space (now Astrium-SAS, Toulouse). Following the approval of *Gaia*, ESA established, in June 2001, sixteen scientific working groups to support the development of the satellite and to prepare for the scientific analysis of the data. One of those groups was charged with the optimization of the spectrograph, named the 'radial velocity spectrometer' (RVS), with respect to the *Gaia* science case. During the following 18 months, the RVS Working Group, with the support of Astrium, reviewed and refined the scientific objectives and priorities for the spectrograph, assessed its performance and compared the advantages and disadvantages of several potential RVS configurations. The scientific requirements and the technical constraints converged toward a refined scientific case and a new spectrograph concept in November 2002. The main modification with respect to the Matra Marconi design is the increase of the resolving power. A broader scientific case has also been associated with the revised configuration of the spectrograph. The acquisition of sufficiently accurate radial velocities for the largest possible sample of stars remains the key scientific objective of the RVS. Radial velocities are fundamental for the proper understanding of the Milky Way structure, origin and history. However, the increased resolution will make it possible, without affecting the radial velocity performance, to address a wide variety of issues in stellar physics: binarity, evolution, rotation, pulsation and variability, atmospheric chemistry, mixing processes and abundance peculiarities.

The RVS science case and general characteristics (e.g. spectral resolution, wavelength range) have now been defined. The more detailed design features (such as the number and type of CCDs) remain to be confirmed. This paper presents the revised and optimized baseline of the RVS: instrument concept (Section 2.1), optical (Section 2.2) and focal plane (Section 2.3) characteristics. Although the instrument concept is expected to evolve in future phases, it should remain broadly within the parameters described here. This paper also presents the RVS calibration (Section 2.4) and observational (Section 2.5) strategies. Finally, it reviews the stellar and interstellar parameters that will be provided by the RVS spectra, namely, radial (Section 3.2) and rotational (Section 3.4) velocities, atmospheric parameters and individual abundances (Section 3.3) as well as interstellar reddening (Section 3.5).

The *Gaia* spectroscopic survey is expected to lead to major improvements in our understanding of the kinematical, dynamical and chemical structure and history of the Milky Way, as well as in our comprehension of stellar physics and evolution. Moreover, it will be ideally suited to the identification and characterization of multiple

systems. The expected scientific harvest is discussed in a companion paper (Wilkinson et al. 2004).

2 RVS DESIGN

2.1 Instrument concept

The RVS is an integral field spectrograph: it uses neither slits nor fibres, but disperses all of the light entering its $2.00^\circ \times 1.61^\circ$ field of view. As with the other *Gaia* instruments, it will continuously and repeatedly scan the sky, observing each object, on average, at 102 successive epochs (see Section 2.5).

The choice of the spectrograph wavelength range ([848, 874] nm: Munari 1999) was motivated by a number of considerations. It is close to the peaks of the energy distributions of the RVS principal targets: G- and K-type stars. In F, G and K stars, there are three strong core-saturated ionized calcium lines in this range, which allows the measurement of radial velocities even at very-low signal-to-noise ratios (i.e. $\sigma\ Vr \simeq 15$ km s^{-1} at $S/N \simeq 1$ per pixel, for a K1 V-type star – see Section 3.2) as well as in very metal-poor stars. In early-type stars, this spectral region is dominated by lines of the hydrogen Paschen series, which are visible even in very rapidly rotating stars. It contains a diffuse interstellar band (DIB), located at 862.0 nm, which appears to be a reliable tracer of interstellar reddening (Section 3.5): this will be used, together with the photometric data, to derive a three-dimensional map of Galactic interstellar extinction. In addition, the extinction in the RVS domain will roughly be a factor of two smaller than in the V band. This will allow the probing of the Galactic disc over greater distances than would be feasible at 550 nm. Finally, this spectral range is almost free of telluric absorption features and is therefore usable from the ground for pre-launch preparatory (and possible complementary, post-mission) observations (Section 3.1).

In its original conception, the spectrograph had an effective resolving power of $R = \lambda/\Delta\lambda = 5750$. During the 18 months of the optimization phase (June 2001–November 2002) the RVS working group compared the merits and drawbacks of a broad range of resolutions from $R = 5000$ to 20 000. The obvious advantage of the 'high' resolutions is that they carry more spectral information than the 'low' ones. The 'weak' lines are sharper, the contrast between lines and continuum is better and the rate of line blending is lower. Therefore, high-resolution spectra provide more accurate diagnostics for the determination of the stellar parameters (e.g. radial and rotational velocities, atmospheric parameters – see Section 3) of most stars except the 'faintest'.[1] Moreover, for $R \geqslant 10\,000$, numerous lines contained in the RVS infrared wavelength range are unblended and it becomes possible to determine the individual abundances of several chemical species and in particular of alpha elements (e.g. magnesium, silicon – see Section 3.3). However, the 'high' resolutions also present a drawback. The RVS is an integral field spectrograph. As a consequence, in regions of high stellar density, the spectra of neighbouring sources will overlap and the mean rate of overlap grows linearly with resolution. Numerical simulations have shown that it will be possible, to a certain extent, to deconvolve the stacked spectra (Zwitter 2003) – see Section 3.2. Even so, in very-crowded areas the faintest sources will be lost in the noise. In those very-dense regions, the limiting magnitude that the RVS can reach is a decreasing function of the resolution.

After extensive consideration within the working group of the advantages and disadvantages of resolving powers between $R = 5000$ and 20 000, a resolving power $R = 11\,500$ was shown to be optimal for the fulfilment of *Gaia*'s scientific objectives. This resolution will allow the radial velocities of late-type stars to be determined with a precision $\sigma\ V_r \leqslant$ 10–20 km s^{-1} up to $V \simeq$ 17–18 (reaching a precision of the order of 1 km s^{-1} or better for the brightest targets), over about 90 per cent of the sky (Section 3.2). The rate of spectral overlap will be lower at $R = 11\,500$ than at higher resolution, thereby allowing the RVS to probe fields of higher stellar density. Moreover, with the resolution $R = 11\,500$ it will be possible to study the chemical pattern of the sources up to $V \simeq$ 12–13 (Section 3.3), while a lower resolution $R = 5750$ did not allow the derivation of individual abundances because of too much line blending and insufficient contrast between lines and continuum. Table 1 summarizes the global characteristics of the RVS.

Table 1. Summary of the general characteristics of the RVS.

Spectrograph type	Integral field
Observing mode	Scan mode
Field of view size	$2.00^\circ \times 1.61^\circ$
Wavelength range	[848, 874] nm
Resolving power ($R = \lambda/\Delta\lambda$)	11 500
Dispersion orientation	along scan
Integration time (per transit)	99 s

2.2 Optics

Gaia will scan the sky with three telescopes. Two of them illuminate the astrometric focal plane (which also contains the broad-band photometric detectors). The third one, the Spectro telescope, is shared by the RVS and the medium-band photometer. The viewing directions of the three telescopes are located in the same plane.

The Spectro telescope, which illuminates both the RVS and the medium-band photometer is made of three silicon carbide (SiC), off-axis, rectangular mirrors. It has an entrance pupil of 0.25 square metres and a focal length of 2.1 m. The 11 medium bands of the photometer cover a wavelength range from the near UV ($\simeq$300 nm) to the near infrared ($\simeq$1000 nm). The mirrors are coated with aluminium which, unlike other metals, exhibits a reflectivity greater than 85 per cent over the whole photometer wavelength range.[2]

Two optical configurations remain under consideration for the RVS. The first, proposed by R. Bingham, is based on the Offner Relay concept (see Reininger 1994 for earlier work on this concept). It is made of three mirrors: two concave (the primary and tertiary mirrors) and one convex (the secondary mirror). The wavelengths are dispersed by a grating ruled on the secondary mirror. The second optical configuration being considered follows a classical arrangement:

(i) a dioptric collimator, which parallelizes the light rays coming from the same field point so that they enter the disperser with the same incident angle;

(ii) a dispersive element: a grism; and

(iii) a dioptric camera, which refocuses the dispersed image on the detectors.

[1] The total read-out and background noise, summed over the 26 nm of the spectrum, increases with the number of samples and therefore with the resolution. For the very-faint stars, the advantages from the larger amount of spectral information is offset by the higher noise levels.

[2] The reflectivity of silver drops very rapidly below $\simeq$350 nm.

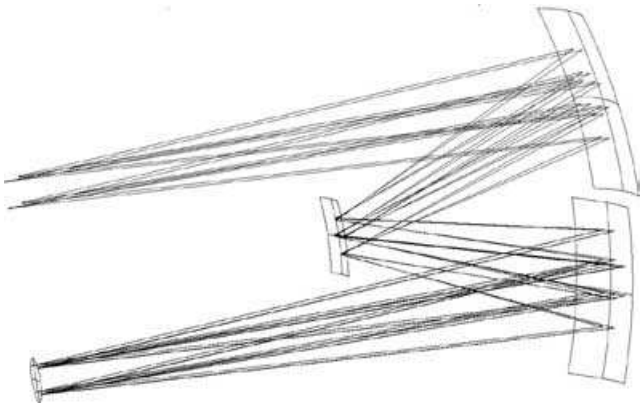

Figure 1. First optical configuration: Offner relay. The spectrograph entrance plane (telescope focal plane) is located in the upper left corner. The RVS focal plane is represented by the ellipse in the lower left corner. The dispersive element, a grating, is ruled on the secondary mirror (centre).

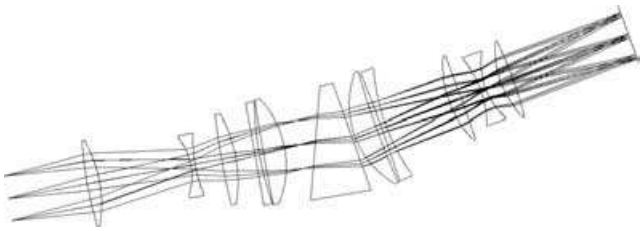

Figure 2. Second optical configuration: dioptric system. The spectrograph entrance plane (telescope focal plane) is on the left side of the figure. The RVS focal plane is represented by the thin line on the right of the figure.

Figs 1 and 2, respectively, show the two possible designs.

In both configurations, a filter blocks the secondary orders and restricts the RVS wavelength range to the adopted domain: [848, 874] nm. The location of the filter has not yet been decided. For the dioptric option, two locations have been proposed: just before the grism or just before the CCD plane. The first option would limit the amount of parasitic light due to secondary reflections on the filter. In the second case the filter would add more effectively to the radiation shielding protecting the detectors.

The spectral dispersion is oriented along the scan direction. The choice of the orientation of the spectra has been partly driven by the shape of the CCD pixels. Because of manufacturing constraints, the pixels are rectangular: narrower in the along-scan direction than in the across-scan direction (see Section 2.3). Therefore, for the same resolution $R = 11\,500$ and sampling (the spectra are sampled at 2 pixels per resolution element), the along-scan orientation of the spectra requires a smaller dispersive power for the grism than the across-scan orientation. In this orientation, the scan law (Section 2.5) acts to broaden spectra in the spatial direction, rather than in the spectral (which would lead to a reduction in spectral resolution). The along-scan orientation also ensures that the spectra of stars located close to the upper or lower boundary of the field of view will not extend beyond the edge of the CCDs.

2.3 Focal plane

The Spectro telescope illuminates three different instruments located in two distinct physical planes. The RVS sky-mapper (whose role is described in Section 2.3.1) and the photometric instrument

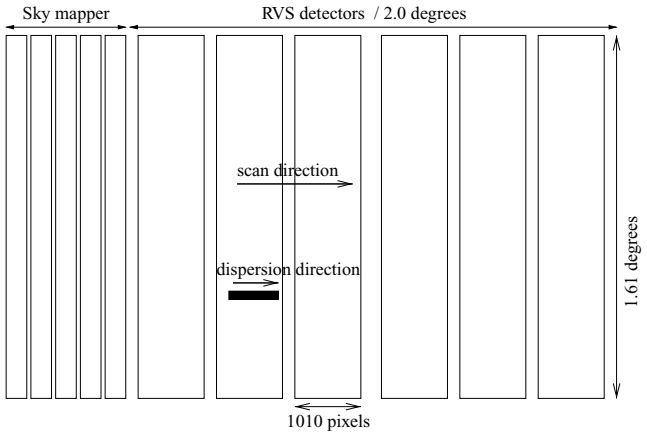

Figure 3. Schematic view, projected on the sky, of the RVS sky-mapper (left) and of the RVS detectors (right). In this figure, the five sky-mapper CCDs are represented side-by-side. In practice they could be mixed with other detectors with different functions (e.g. photometric detectors).

are located at the telescope focus. The RVS CCDs are located at the spectrograph focus. As shown in Fig. 3, the RVS sky-mapper (RVSM) field of view precedes that of the RVS detectors (with respect to the scan orientation).

2.3.1 Radial velocity spectrometer sky-mapper

Unlike *Hipparcos*, *Gaia* will not rely on an input catalogue. The satellite will continuously scan the sky and the sources will be detected on-board in real time by dedicated instruments. In the case of the RVS, this role will be devolved to the RVSM. Subsequently, in order to save telemetry, only the RVS pixels illuminated by a spectrum are transmitted to the Earth.

The RVSM is illuminated in undispersed light. In the current baseline,[3] it is composed of 5 CCDs. Four CCDs are illuminated in white light (to maximize the number of photons collected and increase the detection limit) and one is coated with a red filter (see below). In order to follow the scanning motion of the satellite, the five CCDs are operated in Time Delay Integration[4] (TDI) mode and read continuously. The data from the white-light illuminated CCDs are analysed on-board in real time by a source detection and centroiding algorithm. The detection diagnostics coming from these CCDs are compared in order to reject false detections (e.g. cosmic rays, CCD defects). The centroiding information from the validated detections is used to predict the location and readout times of the spectra on the RVS detectors.

The wide field of view of the RVSM will allow the detection algorithms to identify fast moving objects (i.e. solar system minor bodies and in particular the Near Earth Objects – NEO) and to derive a first estimate of their along- and across-scan motions. The observability of NEOs by *Gaia* is discussed in detail in Mignard (2002).

The fifth CCD will use the same filter as the RVS. This CCD will be used to derive the magnitudes of the sources in the RVS band and to map the sky background with a spatial resolution of $\sim$30 arcsec. In

[3] The number of RVSM CCDs is still under consideration and is subject to change.

[4] The charges are 'continuously' transferred from pixel column to pixel column, in order that they 'follow' the sources in their motions across the field of view.

fields of high stellar density, the RVS band magnitudes are required to disentangle overlapped spectra during the subsequent processing on the ground (see Section 3.2.2).

2.3.2 *Spectrograph focal plane*

As shown in Fig. 3, the 2.0-deg width of the RVS field of view is filled by six CCDs.[5] The design of the RVS focal plane assembly was driven mainly by the issue of the motion of the spectra across the RVS field of view. Because of the *Gaia* scan law (Lindegren 1998), there is a periodic drift of the spectra in the across-scan direction. The transverse velocity of the spectra follows a sine law of period 6 h (the spacecraft spin period). Its mean semi-amplitude is 0.168 arcsec s^{-1}, but this semi-amplitude itself varies on a 6 month time-scale from 0.163 to 0.174 arcsec s^{-1} because of the eccentricity of the Earth's orbit. This means that there is a spatial smearing of the spectra, up to $\simeq$20 arcsec ($\simeq$14 pixels) for a transit across the 2-deg width of the RVS focal plane.

Such spatial smearing is prohibitive in terms of loss of signal-to-noise ratio (since the region from which the spectrum is extracted will be larger and will hence contain more background) and substantially enhances the problems arising from overlapping spectra. Several approaches have been identified and compared to minimize this smearing.

In one approach, a mechanism was envisaged to rotate the detector focal plane to compensate for the transverse motion. Other items that could be actuated instead include the dispersing element or any pair of fold mirrors in the optical path. Besides the inherent complexity, the difficulty with this solution is the requirement that the generation of disturbing torques and variable thermal dissipation within the satellite (which would particularly affect the astrometric measurements) should be kept extremely low.

The second approach is to permit the transverse motion, but to split up the focal plane into smaller detector subunits in the scan direction. The transverse drift per observation (i.e. per CCD) is limited by the shorter exposure time per detector. The total number of pixels in the focal plane, as well as the total exposure time per transit (summed over the smaller detector subunits), is kept unchanged. Assuming six CCDs (and 16.5-s crossing time per CCD), the maximum transverse drift per observation is $\simeq$3 arcsec ($\simeq$2 pixels). This is the technique used in the astrometric payload. The absence of an actuation mechanism is an advantage, but the main consequence of this solution is an increase in the number of readouts for a spectral scan, causing reduced performance because of an increase in the readout noise: the instrument performance is readout-noise limited. This drawback could be minimized through the use of innovative detector technologies (L3CCDs) which exhibit very-low readout noise and by careful design of the detector electronics.

The tilt mechanism and the six L3CCD configurations yield similar performances. The second option (6 L3CCDs) was ultimately adopted because of its lower technical complexity and failure risk. The characteristics of the RVSM and RVS detectors are summarized in Table 2.

One further possible solution is elegant but presently unproven in the context of the RVS. This would be to move the signal 'diagonally' within the detector by means of specialised structures on the CCD itself (2-dimensional clocking), thus compensating for the across-scan drift. This solution could also be effective in compensating for the optical distortion. While this technology still needs to be validated for space applications, it has begun to be used in ground observations (Howell et al. 2003). The use of 2D clocking CCDs for the RVS instrument is under evaluation. This solution will be reconsidered for inclusion in the baseline at the end of phase B1 (end of first quarter 2005).

[5] The number of RVS CCDs is still under consideration and is subject to change.

Table 2. Summary of the RVSM and RVS characteristics. The CCD dimensions and total noise are given for one CCD. The overall efficiency of the RVSM is given for the CCD coated with the RVS filter. The overall efficiency includes the telescope reflectivity, the optics (RVS only), grism (RVS only) and filter transmissions and the CCD quantum efficiency (QE).

	RVSM	RVS
Type of CCD	'classical'	L3 CCD
Operating mode	TDI	TDI
Number of CCDs	5	6
CCD dimensions (pixels)	336 × 3930	1010 × 3930
CCD dimensions (degrees)	0.09 × 1.61	0.28 × 1.61
Exposure time/CCD (s)	5.5	16.5
Pixel size (microns)	10 × 15	10 × 15
Pixel size (arcsec)	0.98 × 1.47	0.98 × 1.47
CCD total noise (e^-/pixel)	9	2
CCD QE ($\lambda = 500$ nm)	66 per cent	– –
CCD QE ($\lambda = 700$ nm)	92 per cent	– –
CCD QE ($\lambda = 860$ nm)	71 per cent	71 per cent
Filter transmission	85 per cent	85 per cent
Overall efficiency ($\lambda = 860$ nm)	40 per cent	21 per cent

2.3.3 *RVS observations*

The RVS will be operated in TDI scan mode. Therefore, the raw RVS observations will appear as a 'never-ending' strip of (spectrally) dispersed sky. However, in order to save on the telemetry budget, only the parts of the raw observations containing spectra will be downloaded to the Earth.

Fig. 4 shows snapshots of simulated raw RVS observations for high (top) and low Galactic latitudes (bottom). The images on the left and on the right contain the same stars and only differ by the luminosity scales used to code the number of photo-electrons recorded per pixel (and per transit). The left-hand side images are coded with an inverse linear luminosity scale. In the right-hand side images, the pixels whose intensities are in the range [1, 125] e^- are coded with an inverse linear luminosity scale and the pixels which exceed 125 e^- are coded in black.

These images have been generated taking into account the main RVS characteristics: spectral resolution, instrumental throughput efficiency, filter function, spatial and spectral point-spread-function (PSF), detector pixel dimensions, photon noise, readout noise, a model for the Zodiacal light contribution and the spatial smearing due to the scan law. The images have been generated down to $V = 20$ using the star density counts as function of Galactic latitude from table 6.6 of the ESA (2000) report and the distribution of spectral types as given in their table 6.4. The star positions have been generated randomly for this assumed stellar density. Spectra of the appropriate brightness and spectral type have been simulated by scaling model spectra taken from the library of Zwitter, Castelli & Munari (2003, 2004). The RVS field of view simulator is accessible and can be run on-line via the simulator web site: http://www.mssl.ucl.ac.uk/gaia-rvs/simulator.html.

What is immediately clear from the simulated images in Fig. 4 is the effect of the overlapping of spectra in low Galactic latitude

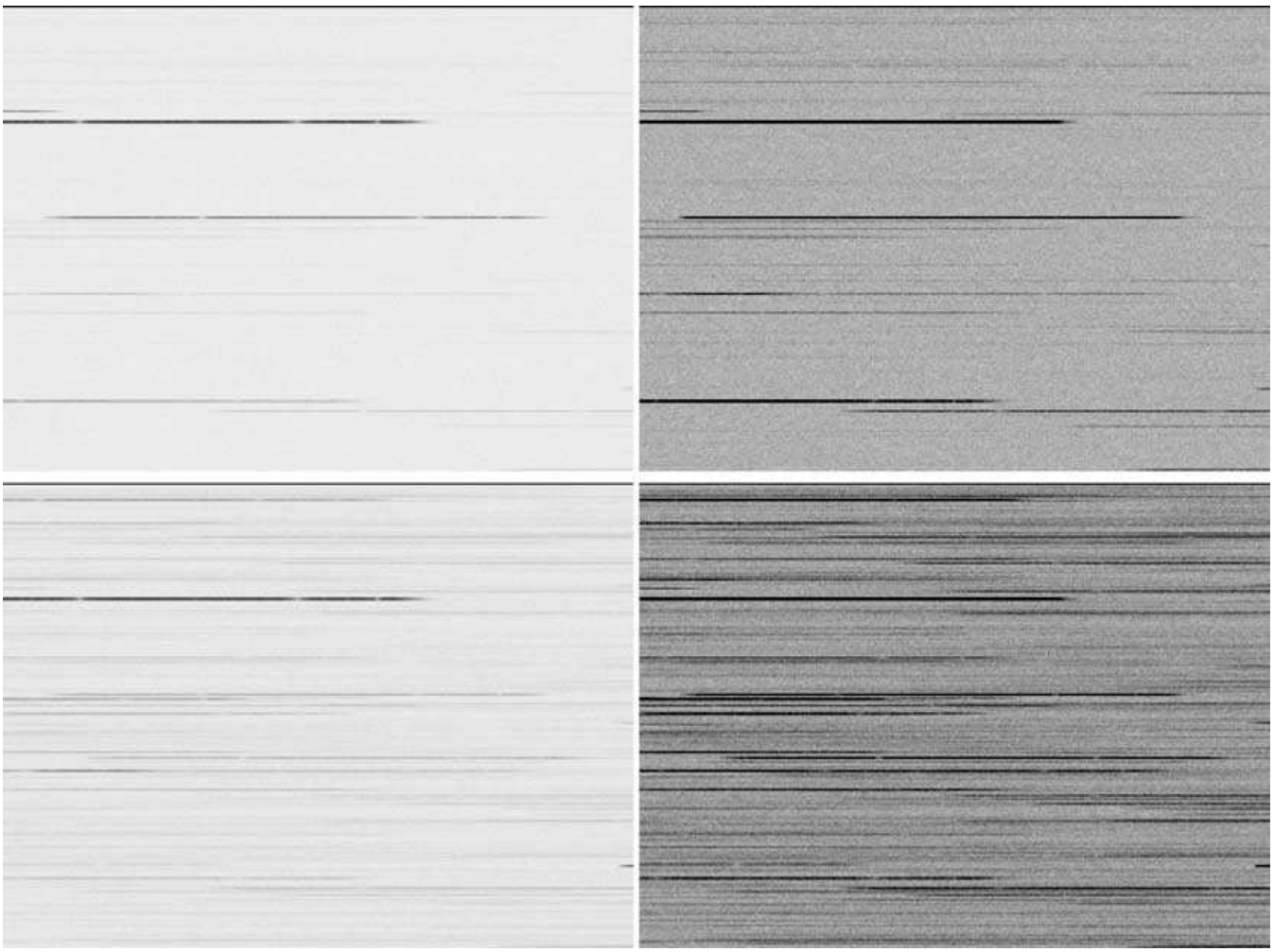

Figure 4. Simulated *Gaia*-RVS images for high Galactic latitudes (top) and $|b| \leqslant 5^\circ$ (bottom), in linear scale (left) and in 'thresholded' linear scale (right). The images are generated for one transit of the focal plane of six CCDs, each with a readout noise of $2e^-$.

fields. Less evident, but partly visible in the right-hand side images, is the number of spectra at low light levels in these images (at the $V = 17.5$ limit, spectra have accumulated less than 1 photon per pixel per transit). Indeed, the spectra visible on the right-hand side of Fig. 4 are all from stars with $V \leqslant 15$. This emphasizes the extent to which the readout noise (2 e^- per pixel per CCD) dominates the signal at the limiting magnitude, except in the Galactic plane where the dominant background is due to faint stars. Therefore, the derivation of radial velocities at the limiting magnitude will be possible only after the co-adding of all of the scans of a given target taken by the end of the mission. This has critical implications for the data-handling, compression and transmission and rules out the possibility of using lossy compression algorithms in transferring the data to the ground.

In Fig. 4, the background light (here only zodiacal light) displays no spectral signature. This will be the case in all the regions of the sky where the background light surface brightness is uniform on an angular scale of a few arcmin: the spectral information will be smoothed by the slow variation of this source over the field of view.

The simulated images differ from the actual RVS raw observations in that they do not yet include the effects of pixel-to-pixel variability within the detector, any cosmetic defects in the detectors, or cosmic rays. In addition, they do not include the 'small' effect of spectral and spatial smearing due to the 'small' distortions from the telescope plus spectrograph optics, nor the effects of co-adding the signal from several detectors that might not be perfectly aligned. In addition, the spectral catalogue contains only 'normal', single stars.

2.4 Calibration strategies

The RVS, as well as the other *Gaia* instruments, presents several peculiarities with respect to classical ground-based instruments: it will scan the sky continuously with (hopefully) no interruption during the 5-yr mission; it will observe $\sim$100–150 $\times$ 10^6 stars; each star will be observed a large number of times; the instrument will be extremely optically and mechanically stable. All these items support the idea that the RVS instrument could be self-calibrated using a global iterative approach.

The principle of the global iterative calibration is to use an iteratively self-selected sample of 'well-behaved' stars (i.e. sufficiently bright; astrometrically, photometrically and kinematically stable over successive observations; of a spectral type well-suited for the wavelength calibration) to derive, iteratively, the radial velocities of the iteratively selected stars, calibrate the wavelength scale and calibrate the instrument response and geometry.

The calibration process will use the information provided by the other *Gaia* instruments: very-accurate source positions, very-good knowledge of the satellite attitude and of the magnitudes, colours

and atmospheric parameters of the sources. Pre-flight calibrations, as well as ground-based radial velocity standards (selected, for example, from among the Solar-type stars surveyed for extra-solar planets), will be used to initiate the iterative process. With the progress of the mission, *Gaia* will iteratively select thousands of appropriate standards, which will complement the ground-based standards and will provide a very-constrained grid in the spatial and temporal dimensions. Finally, the ground-based standards will fix the zero point of the radial velocities.

The full-precision results will be obtained after completion of the observations and after convergence of the iterative auto-calibration procedure. The final *Gaia* catalogue should be available a few years after mission end, i.e. around 2017–2020. Intermediate releases, of lower precision than the final catalogue, could be envisaged a few years after launch, e.g. ∼2012–2014.

The procedure described above is presently the baseline for the calibration of the RVS and in particular its wavelength calibration. Studies are also in progress to assess whether complementary techniques could be used. The slit-less, objective-prism-like modus operandi of the *Gaia* spectrograph prevents the use of standard ground-based calibration techniques, involving lamps or sky lines. The only possibility to *mark* wavelengths on *Gaia* spectra is to absorb selective wavelengths. Should it emerge during the RVS final system design that it would be a useful tool to implement, an absorption cell could be inserted in the optical chain, filled with an appropriate absorbing medium able to mark strong and widely spaced absorption lines away from those of major astrophysical relevance. Efforts to identify an absorbing medium appropriate for the *Gaia* operating conditions are underway (Desidera & Munari 2003; Pernechele & Munari 2003). Alternatively, a bundle of multimode optical fibres carrying suitable Bragg gratings, inserted in the collimated beam, could be considered. These alternative ways of wavelength calibrating *Gaia* spectra would probably be of greater interest in the pre-, during- and post-flight ground-based observations, when the maximization of the science exposure time and the increase of the accuracy are particularly sought after. Particularly promising in this respect are the fibre Bragg gratings that are suitable for mass production.

2.5 Observation strategy

The *Gaia* satellite will scan the sky continuously during the 5-yr mission. As in the case of its precursor *Hipparcos*, a uniform revolving scan has been proposed for *Gaia* and parameters for the scanning law were calculated to produce a smooth sky coverage and achieve the best accuracy on the measurements of the astrometric parameters.

The *Gaia* nominal scanning law (NSL) is described in Lindegren (1998). Some of its parameters have been modified in spring 2002 to take into account changes in the payload design due to the change of launcher from Ariane V to Soyouz-Fregat.

Gaia will rotate around its z-axis with a uniform velocity of $\omega = 60$ arcsec s^{-1} so that each instrument will scan a great circle on the sky in 6 h. The rotational axis itself precesses at a constant angle of 50 deg around the direction from the satellite to the centre of the Sun. The mean speed of the rotational z-axis on the sky, in units of the apparent Sun speed, is equal to 4.095; this leads to a mean number of 5.200 (overlapping) precession loops of the z-axis on the sky per year, each loop being covered in ∼70 d. A complete sky coverage is achieved in one year through motion of the axis of the precession cone (which points towards the Solar centre) along the ecliptic.

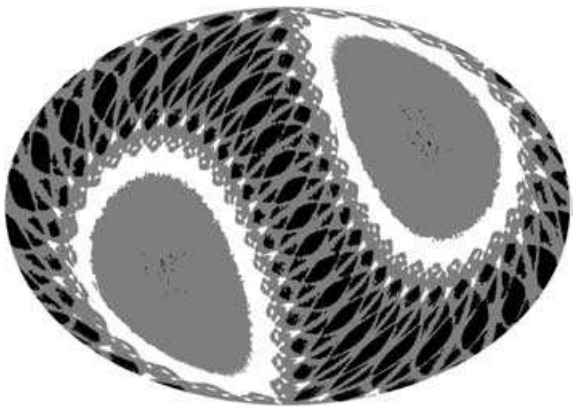

Figure 5. Number of transits through the RVS-field of view versus Galactic coordinates for the 1800-d *Gaia* mission. There are three 'grey' levels: $\leqslant$80 transits (black), between 80 and 120 transits (grey) and $\geqslant$120 transits (white).

The NSL makes it possible to predict the attitude of the satellite as a function of time throughout the mission. Using the attitude parametrisation of *Gaia*-NSL based on the quaternion formalism derived by Lindegren (2000) and the FORTRAN code he provided (Lindegren 2001), the total number of transits during the assumed 5-yr mission (arbitrarily starting from J2000) was computed as function of position on the sky for integer values of Galactic longitude and latitude. The number of transits versus Galactic coordinates are plotted in Fig. 5. A similar figure, showing the number of RVS transits as function of ecliptic coordinates, is presented by Pourbaix & Jancart (2003). According to the position on the celestial sphere, the number of transits for the RVS instrument ranges from 54 to 239, with a mean value (averaged over the sky) of 102.

The RVS will provide radial velocities for late-type stars up to magnitude $V \simeq 17$–18 (see Section 3.2). The star count model of Chen (1997) has been used by Torra et al. (1999) (updated values are given in ESA 2000) to evaluate the number of stars to be observed by *Gaia* as function of magnitude, stellar population, stellar type and Galactic coordinates. The model predicts that 100–150 million stars will be observed up to magnitude $V = 17$–18. Approximately 80 per cent of those stars will belong to the thin disc, $\simeq$15 per cent to the thick disc and $\simeq$5–10 per cent to the halo and the bulge. The majority ($\simeq$70 per cent) of RVS targets will be G- and K-type stars.

3 STELLAR AND INTERSTELLAR PARAMETERS

3.1 Spectra

In the RVS wavelength range, [848, 874] nm, the spectra of F-, G- and K-type stars are dominated by the ionized calcium triplet (849.80, 854.21, 866.21 nm). Although the strength of the triplet lines decreases with increasing gravity, it nevertheless remains very strong in dwarf stars: their equivalent widths are larger than 0.3 nm for stars of spectral type F8 V to M6 V. The triplet is non-resonant and therefore will not be affected by contributions from the interstellar medium. In addition to the calcium triplet, the RVS spectra of late-type stars will also contain numerous unblended weak lines of astrophysical interest and in particular alpha-elements like Si I or Mg I. In the coolest stars, CN and TiO molecular transitions are visible, but no strong molecular bandhead is present.

In early-type stars, the strongest features are the Paschen lines whose equivalent widths are strongly anti-correlated with gravity.

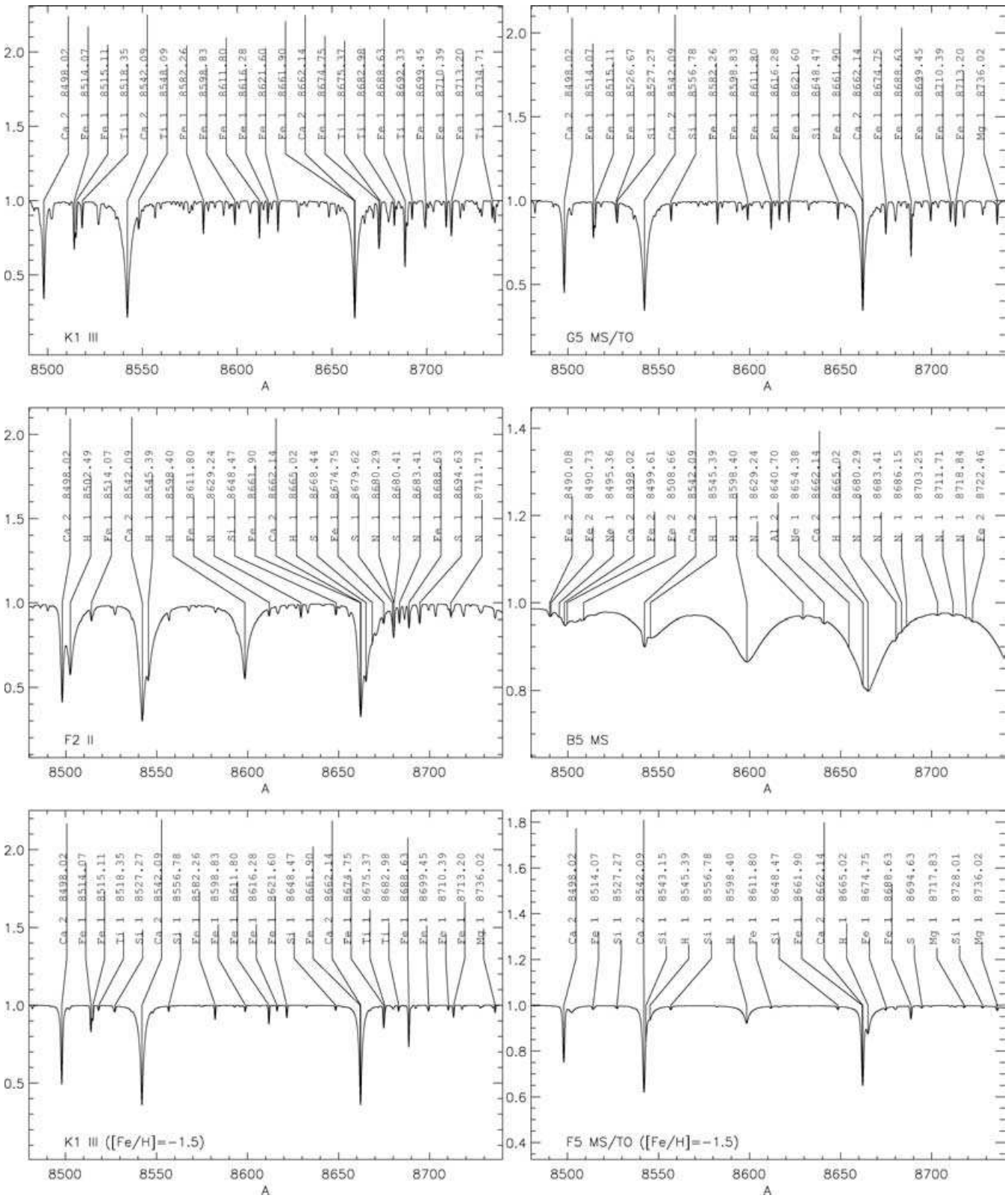

Figure 6. Six examples of RVS-like spectra. The panels show four solar-metallicity stars: G5 turn-off (top left), K1 III (top right), F2 II (middle left), B5 main sequence (middle right); and two metal-poor stars: F5 turn-off (bottom left) and K1 III (bottom right). See Table 3 for details.

The spectra of hot stars also exhibit some other strong (e.g. Ca II, N I) and weak (e.g. He I, He II) lines.

In addition to the stellar features, the RVS wavelength range contains a diffuse interstellar band (862.0 nm) which appears to be a reliable tracer of interstellar reddening (see Section 3.5).

Fig. 6 shows examples of synthetic RVS-like spectra for 6 representative tracers of Galactic structure: a K1 III star and a G5 main

Table 3. Parameters of the six representative tracers of Galactic structure plotted in Fig. 6.

	$T_{\rm eff}$	$\log g$	[Fe/H]	[α/Fe]	$v \sin i$
K1 III	4 500	2.0	0.0	0.0	5.0
G5 MS/TO	5 500	4.0	0.0	0.0	5.0
F2 II	7 000	1.0	0.0	0.0	20.0
B5 MS	15 000	4.5	0.0	0.0	50.0
K1 III	4 500	2.0	−1.5	+0.4	5.0
F5 MS/TO	6 500	4.0	−1.5	+0.4	20.0

sequence/turn-off (MS/TO) star of solar metallicity (typical of the disc); an F2 supergiant and a B5 MS star (tracers of spiral structure); a K1 III star and an F5 MS/TO star, both metal-poor (typical of the halo). The parameters of the 6 stars are summarized in Table 3. They have been computed using the VALD atomic data (Piskunov et al. 1995; Ryabchikova et al. 1999; Kupka et al. 1999), the Kurucz atmospheric model (Kurucz 1993a) and N. Piskunov's SYNTH program (Piskunov 1992). All models and spectra have been computed assuming a micro-turbulence velocity of 2 km s^{-1} and plane-parallel static atmospheres.

The easy accessibility from the ground of the *Gaia* wavelength range was one of the factors emphasized by Munari (1999) when proposing the [848–874] nm interval, which was at that time also discussed within the *Gaia* Science Advisory Group as one of the possible wavelength ranges for the mission's spectrograph. This interval is also remarkably clear of telluric absorption, unlike the rest of the $\lambda \geqslant 670$ nm far-red optical region.

This allows an intensive observational campaign to be conducted with ground-based telescopes with the aim of deepening our knowledge of this wavelength interval at spectral resolutions equal to, or larger than, the 11 500 foreseen for *Gaia*. By the time that *Gaia* will start to deliver its spectral data, it is to be anticipated that it will become the reference interval for classification and analysis. A wide range of spectroscopic follow-up options will be open to ground-based telescopes, including either a similar observing strategy to that of *Gaia* but to fainter limits, or the extension of the time coverage of variable phenomena.

Inspection of the Asiago Data base of Spectroscopic Data bases (ADSD) (Sordo & Munari 2003; Sordo & Munari, in preparation), listing 259 atlases for the optical region, returns 12 spectral atlases containing more than 15 objects over the *Gaia* wavelength interval at a resolution larger than 3 000. These 12 atlases offer some insight into the appearance of real stars in this wavelength region, including peculiar types, and the cooler spectral types (F,G,K) that will dominate the field star population at the *Gaia* magnitudes are particularly abundant. The characteristics of the 12 atlases are summarized in Table 4.

No special observational effort appears to be required to assemble new spectral atlases surveying normal stars over the HR diagram in this spectral region. However, more work on metal-poor, peculiar and molecular-band stars (M, C, S) can and should be carried out.

3.2 Radial velocities

3.2.1 Performances

The initial motivation for the implementation of a spectrograph on board *Gaia* was the acquisition of radial velocities. Their determination has, to a large extent, driven the definition and optimization of the characteristics of the RVS. Throughout the definition

Table 4. Spectral atlases with a minimum sample of 15 stars and a resolving power larger than 3000 over the *Gaia* 848–874 nm spectral range. The columns give the resolving power (R.P.), the number of stars included and the range of their spectral types.

Atlas	R.P.	N	Spec. type
Andrillat, Jaschek & Jaschek (1995)	3 000	76	O5–G0, pec
Cenarro et al. (2001)	5 000	706	O6–M8
Carquillat et al. (1997)	6 500	54	A2–M4, C, S
Valdes et al. (2004)	7 200	1273	A0–M8, C, S
Serote Roos, Boisson & Joly (1996)	8 000	21	B3–M5
Fluks et al. (1994)	8 600	22	M III
Montes, Ramsey & Welty (1999)	13 000	132	F0–M8
Munari & Tomasella (1999)	20 000	130	O4–M8
Marrese, Boschi & Munari (2003)	20 000	94	F2–M7
Pavlenko, Marrese & Munari (2003)	20 000	24	Carbon
Munari (2003)	20 000	17	pec
Montes & Martin (1998)	55 000	48	F5–M8

phase, studies were conducted to evaluate the performance of the different proposed configurations. Those studies all rely on similar Monte Carlo approaches to derive the RVS radial velocity precision: cross-correlating a large number of RVS-like spectra, either observed (Munari, Agnolin & Tomasella 2001; David 2001) or synthetic (Katz 2000; Katz et al. 2002; David 2002a,b; Zwitter 2002; Munari et al. 2003) against suitable templates.

Subsequently, the simulations have been re-run to evaluate the performance of the RVS adopted baseline as a function of magnitude and for the 6 representative tracer populations listed in Table 3. In addition, for each of the three spectral types, F2 II, B5 MS and F5 MS/TO, which could present high rotational velocities, two projected rotational velocities have been considered: a 'low' and a more 'typical' value (see Table 5).

To generate RVS-like observations, Kurucz (1993b) synthetic spectra have been convolved to the RVS spectral resolution, normalised to the star magnitude (according to its atmospheric parameters), sampled (assuming two pixels per PSF full width at half maximum – FWHM) and degraded with photon, background and detector noise, using a simulator of the RVS instrument (Katz, in preparation). The simulations took into account zodiacal light and faint background stars (assuming a total surface brightness of $V = 21.75$ mag arcsec^{-2}), the telescope pupil area, the overall instrument efficiency, the exposure time, the spectral profile perpendicular to the dispersion direction and detector noise.

The performances were derived by Monte Carlo simulations. For each spectral type and magnitude, 1000 or 2000 cross-correlations of RVS-like spectra with Kurucz synthetic templates (convolved at the RVS resolving power) were performed in direct space. In each case, the precision was derived using a robust estimator of the standard deviation of the distribution of (1000 or 2000) estimated radial velocities. After sorting the radial velocities, the standard deviation was estimated using the following formula:

$$\sigma = \frac{V_{\rm R(0.8415)} - V_{\rm R(0.1585)}}{2}. \quad (1)$$

Here $V_{\rm R(0.1585)}$ is the 15.85th percentile of the sorted distribution of radial velocities and $V_{\rm R(0.8415)}$ is the 84.15th percentile of the same distribution. This robust estimator gives low weight to the outliers which appear at the faintest magnitudes (when secondary correlation peaks could be mistaken for the correct correlation peak). Future work will focus on the development of techniques to identify

Table 5. Precision (one sigma error) of the RVS instrument in the derivation of radial velocities as a function of magnitude, for a single observation (top) and at the end of the mission (102 observations: bottom). The performances are expressed in km s^{-1}.

	[Fe/H]	$v \sin i$	Single transit, for $V =$									
		(km s^{-1})	9	10	11	12	13	13.5	14	14.5	15	15.5
K1 III	0.0	5	$\leqslant$1	$\leqslant$1	$\leqslant$1	1.1	2.3	3.1	4.7	7.2	11.5	34.9
G5 MS/TO	0.0	5	$\leqslant$1	$\leqslant$1	1.2	2.1	4.4	6.3	9.7	19.7	>35	>35
F2 II	0.0	20	$\leqslant$1	1.3	2.3	4.3	9.3	14.4	24.3	>35	>35	>35
F2 II	0.0	50	1.3	2.1	3.6	6.5	13.8	21.2	33.4	>35	>35	>35
B5 MS	0.0	50	14.8	25.0	>35	>35	>35	>35	>35	>35	>35	>35
B5 MS	0.0	150	18.3	31.1	>35	>35	>35	>35	>35	>35	>35	>35
K1 III	−1.5	5	$\leqslant$1	$\leqslant$1	1.1	1.8	3.6	5.0	7.5	11.7	26.8	>35
F5 MS/TO	−1.5	20	1.2	1.9	3.2	5.8	12.3	24.3	>35	>35	>35	>35
F5 MS/TO	−1.5	50	2.1	3.4	5.6	10.7	22.3	>35	>35	>35	>35	>35

	[Fe/H]	$v \sin i$	Mission (102 transits – average case), for $V =$									
		(km s^{-1})	12	13	14	15	15.5	16	16.5	17	17.5	18
K1 III	0.0	5	$\leqslant$1	$\leqslant$1	$\leqslant$1	1.1	1.6	2.6	3.8	6.2	10.6	25.5
G5 MS/TO	0.0	5	$\leqslant$1	$\leqslant$1	$\leqslant$1	2.1	3.4	5.0	8.3	16.0	>35	>35
F2 II	0.0	20	$\leqslant$1	$\leqslant$1	2.0	4.8	7.6	12.6	20.8	>35	>35	>35
F2 II	0.0	50	$\leqslant$1	1.3	3.1	7.5	11.4	18.0	29.9	>35	>35	>35
B5 MS	0.0	50	8.2	18.6	>35	>35	>35	>35	>35	>35	>35	>35
B5 MS	0.0	150	10.0	23.5	>35	>35	>35	>35	>35	>35	>35	>35
K1 III	−1.5	5	$\leqslant$1	$\leqslant$1	$\leqslant$1	1.7	2.5	4.1	6.3	10.3	23.4	>35
F5 MS/TO	−1.5	20	$\leqslant$1	1.1	2.6	6.1	9.5	17.3	>35	>35	>35	>35
F5 MS/TO	−1.5	50	1.0	2.0	4.4	10.5	16.9	31.6	>35	>35	>35	>35

and reject these outliers. The fraction of outliers (i.e. the fraction of estimated radial velocities beyond 3 times the estimated dispersion) is, to a first approximation, a function of the estimated dispersion and of the stellar type. For $\sigma = 5$ km s^{-1} there are $\simeq$1.5 per cent and $\simeq$0 per cent outliers, respectively, in the cases of a G5 V star and of a F2 II star. The fractions of outliers become $\simeq$12 per cent and $\simeq$7 per cent, respectively, for $\sigma = 20$ km s^{-1}.

In these simulations, the distributions of estimated radial velocities exhibit no statistically significant bias.

Many small effects still remain to be taken into account in the full assessment of the RVS accuracy budget. These include optical aberration, CCD charge transfer inefficiency, instrument and wavelength calibration. In order to account for these missing effects, a 40 per cent explicit error margin was added to the RVS performances. The radial velocity performances, for single observations and at the end of the mission (after combining the 102 observations collected over the 5-yr mission), are presented in Table 5. It is likely that the second order effects will become very significant or even dominant for sufficiently bright stars, for which the present simulations give 1 km s^{-1} or better performance. For this reason, no values below $\sigma = 1$ km s^{-1} are given in Table 5. Above $\sigma \simeq$ 30–40 km s^{-1} the performance degrades very rapidly as function of magnitude and the estimation of the performance becomes imprecise. As a consequence, no values above $\sigma = 35$ km s^{-1} are given in Table 5.

The precisions given in Table 5 have been evaluated for the average number of observations per star, namely 102 transits. As described in Section 2.5, the number of epochs of observation will vary with Galactic coordinates. As a consequence, the end of mission performances and the range of magnitude probed by the RVS will also vary with Galactic coordinates. As an example, for a G5 MS/TO and for the minimum (54 transits), average (102 transits) and maximum (239 transits) number of observations, a precision of $\sigma \simeq 16$ km s^{-1} is obtained, respectively, for $V \simeq$ 16.65, 17 and 17.45 mag.

Another parameter that varies with Galactic coordinates and that will impact on the RVS performance is the stellar density. This is discussed in the next section.

3.2.2 *Crowded regions*

Because the RVS is an integral field spectrograph, some degree of spectral overlap is unavoidable, even in regions with a low stellar density. Consequently, the background to be subtracted from any spectrum consists not only of the smooth zodiacal light contribution but also of discrete jumpy spectral tracings of (partially) overlapping stars. Fig. 7 depicts examples of such background spectra: on the left, a low-density region (1000 stars deg^{-2} with $V < 17$) typical for the 'high' Galactic latitudes ($|b| \geqslant 30^\circ$) and on the right, a higher density region (6000 stars deg^{-2} with $V < 17$) representative of the range of latitudes: $5^\circ \leqslant |b| \leqslant 10^\circ$.

Overlaps of the brightest background stars are rare and occur only on a small number of transits. Their contribution to the overall background is not, however, negligible and their spectral lines can degrade the accuracies of the radial velocity or other parameters. Fig. 7 shows the background accumulated over the whole mission, excluding transits with overlapping stars brighter than $V = 14$. The loss of integrated signal corresponding to the rejection of the transits containing 'bright' contaminating stars is acceptably low. Bright ($V < 14$) overlappers are present in $\sim$3 per cent (Galactic halo) or $\sim$13 per cent (Galactic plane) of all transits. The bottom panels of Fig. 7 plot individual contributions from the ten strongest overlapping stars fainter than $V = 14$ while the top panels show the background signal, which is the sum of these 10 and several fainter contributions. The fluxes are given in units of the flux from a $V = 17$ K1 V star integrated over the whole mission (102 transits). Note that the accumulated background is very smooth. Lines from individual overlapping stars become diluted by the continuum contributions of other overlapping stars in the same and other transits.

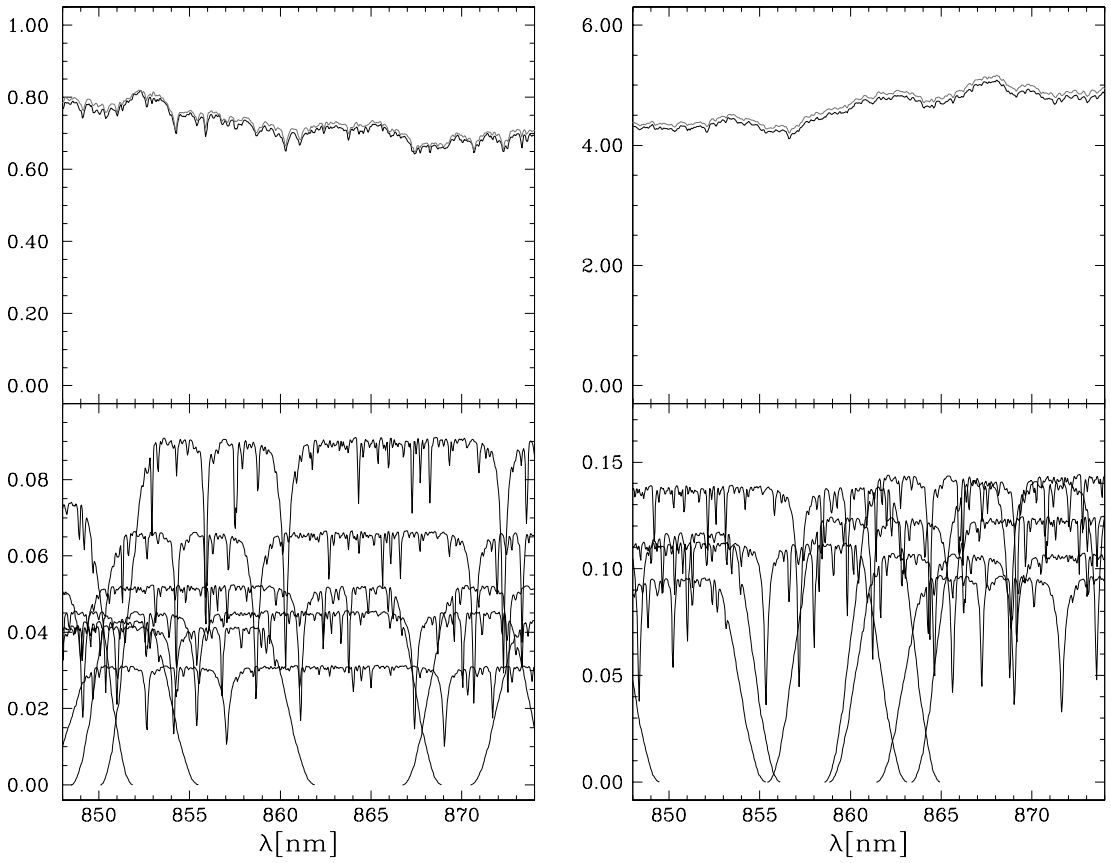

Figure 7. Crowding of stellar spectra in the focal plane of the slitless spectrograph results in spectral overlaps. The left panels depict the typical situation at 'high' Galactic latitudes: 1000 stars deg^{-2} with $V < 17$. The right panels are for a more crowded region near the Galactic plane: 6000 stars deg^{-2} with $V < 17$. The top panels show the background accumulated over the whole mission (for a spectral tracing width of 2 pixels) if the transits with overlaps of stars brighter than $V = 14$ are omitted. The true background is plotted in black (lower line) and the one recovered from the astrometric and photometric information from other instruments aboard *Gaia* in grey (upper line). The bottom panels show, in the same ordinate units as in the upper ones, the contribution to the background of the ten brightest stars fainter than $V = 14$. Ordinates are fluxes in units of the flux from a $V = 17$ K1 V star integrated over the whole mission.

The background can be very well modelled from information that is available from *Gaia*'s astrometric and photometric measurements (stellar positions, magnitudes, rough spectral types and velocities of overlapping stars). In Fig. 7 it is assumed that stellar positions and magnitudes are accurately known, which is certainly true given the excellent astrometric accuracy combined with the photometric and star mapper measurements. Also, spectral information could be derived from photometric observations: in Fig. 7 a mismatch of 250 K in temperature and 0.5 dex in metallicity and gravity are assumed. We note that this is conservative, as the final errors on these parameters are expected to be roughly half these values. If, in addition, some knowledge (provided by the RVS) on the radial velocities of the overlapping stars is assumed, the overall background can be modelled.

From the above paragraph, it would appear that the radial velocities are simultaneously necessary to model both the background and the unknown information one wants to extract from the spectra. One possible approach to solving this problem is to proceed in an iterative way. At each iteration, the 'stacked' spectra are analysed, one by one, from the brightest to the faintest star. The analysis of each spectrum is made of two consecutive steps: modelling and subtraction of the background and then derivation of the radial velocity. On the first iteration, the background of a given star is modelled using the first estimates of the radial velocities of the sources brighter than this star (which have already been analysed) and using only the level and shape of the continua of the fainter stars (whose radial velocities have not yet been estimated). At the end of the first iteration, an estimate of the radial velocity of each of the 'stacked' stars has been derived. The process is then iterated. The new or refined estimates of the radial velocities are used to refine the background modelling which, in turn, is used to refine the estimates of the radial velocities.

The simulations performed to compute Fig. 7 assume that the radial velocities are known with precisions of: $\sigma\ V_{\rm R} = 2$ km s^{-1} at $V = 14$ and 20 km s^{-1} at $V = 17$ (this simulates an intermediate stage of the iterative process). The result of the background modelling (grey lines in the top panels of Fig. 7) is encouraging. First tests based on the background modelling technique (Zwitter 2003) inspire confidence that radial velocities can be obtained from such overlapping spectra with moderate degradation of performance up to $\simeq$20 000 stars deg^{-2} with $V < 17$.

The information obtainable from crowded regions will be worse than for sparsely populated ones. Nevertheless, the overlapping stars degrade the RVS accuracy mainly by increasing the background shot noise level. Such a conclusion is justified if one can rely on accurate knowledge of the flux throughput of the instrument and on accurate spectral modelling of the background stars. In forthcoming studies, we intend to investigate this issue in detail

and, in particular, to implement and test the full iterative analysis process.

3.3 Atmospheric parameters and individual abundances

Gaia will rely on a large variety of observables to classify and parametrize the stars (Bailer-Jones 2002, 2003): distances (and therefore absolute magnitudes), five broad photometric bands, 11 medium photometric bands and $R = 11\,500$ spectra over the wavelength range [848, 874] nm. In this section we focus on the information contained in the spectroscopic data.

The spectral richness of the RVS wavelength range gives a broad diversity of line absorption responses that vary with $T_{\rm eff}$, $\log g$ and $[Z/Z_{\odot}]$.[6] As a consequence, the RVS spectral range contains all the required information to derive the stellar atmospheric parameters.

At present, the spectroscopic determination of the atmospheric parameters requires the micro-turbulence velocity to be constrained. In the future, this *ad hoc* parameter will be replaced by a three-dimensional description of the stellar atmospheric structure (temperature, pressure, etc.) and velocity field.

Many methods have been developed for determining stellar atmospheric parameters from spectra. One widely used technique is detailed stellar spectral analysis. The effective temperature and surface gravity are constrained by requiring that abundances derived from different lines be independent of the line excitation potential (for a given element) and of the element ionization stage. This method (even fully automated) is not suited for the analysis of RVS spectra because of the absence of sets of weak unblended lines from given elements in two different ionization stages, which would allow the ionization equilibrium to be constrained. Alternative techniques have been developed based on automatic comparison using the minimum distance method between measured and synthetic spectral quantities such as the equivalent widths (EWs) of strong lines (Thevenin & Foy 1983). These methods also require a 'good' S/N ratio, which reduces their performance for faint stars.

For this reason, different techniques have been developed in order to analyse spectra of moderate-to-low S/N ratios. In these techniques, the set of EW values have been replaced by the whole spectrum (Cayrel et al. 1991; Thevenin & Jasniewicz 1992; Katz et al. 1998; Allende Prieto 2003), diminishing the effect of a low S/N ratio and producing results comparable with those of a detailed analysis based on spectra with high resolution. Thevenin, Bijaoui & Katz (2003) have used a grid of synthetic spectra to explore the influence of resolution on the recovered atmospheric parameters of late-type stars. They concluded that resolutions $R = 12\,000$ and higher were appropriate to recover the three main atmospheric parameters. Soubiran (2001) has evaluated the performance of the comparison of full spectra using the minimum distance method in the RVS wavelength range and assuming a resolving power half that adopted for *Gaia*. She degraded the observed spectra from the library of Cenarro et al. (2001) to S/N = 20 and compared each spectrum with the rest of the library one by one. The parameters of the stars were recovered with precisions of: $\sigma(T_{\rm eff}) = 275$ K, $\sigma(\log g) = 0.36$ $\sigma([{\rm Fe/H}]) = 0.22$ dex. An S/N of 20 by the end of the mission corresponds to $V \simeq 14.5$ for a K1 III star, $V \simeq 14.0$ for a G5 V star and $V \simeq 13.5$ for an F2 II star. Because of its higher resolution, the RVS performances are expected to be better than this.

Another way to extract the atmospheric parameters is to use Neural Networks (Bailer-Jones 2000). Tests have demonstrated (Bailer-Jones 2003) that using the $R = 5800$ library[7] of Cenarro et al. (2001), $T_{\rm eff}$ can be determined to within 5 per cent, $\log g$ within 0.5 (solar metallicity) to 1.0 (metal-poor stars) and [Fe/H] within 0.3 dex.

Up to $V \simeq 14$–15, the atmospheric parameters will be derived using not only the spectroscopic observations, but also (and jointly) the astrometric and photometric data. The global precision of the atmospheric parameters from *Gaia* should be higher than that estimated from the spectroscopic information alone, which is presented here. The astrometric and photometric observations will also allow the evaluation of the atmospheric parameters of the fainter stars.

For the brightest stars, measurements of equivalent widths and/or synthetic profile fitting will allow the extraction of individual abundances from RVS spectra. The elements concerned are mainly Fe, Ca, Mg and Si for late-type stars F, G and K. The abundances of other elements like N can be derived in hotter stars such as A-type stars. For the cooler stars, K and M types, molecular bands can provide information on C, N or TiO abundances. This raises the possibility of investigations into the chemical evolution of the Galaxy. Owing to the quality of the spectra, the error on the deduced stellar abundance of a chemical element depends on the resolution, the S/N and the spectral sampling on the CCD. Using Cayrel's formula (Cayrel 1988), the error on an equivalent-width measurement of 0.005 nm at a resolution $R = 11\,500$ and for S/N = 50, is 0.0015 nm, corresponding, for this weak line, to an error of 0.13 dex on the abundance. S/N = 50 (at the end of the mission) corresponds to $V \simeq 13$ for G5 V and K1 III stars and to $V \simeq 12$ for an F2 II star.

The RVS spectra will be used, jointly with the photometric and astrometric data, to determine the atmospheric parameters of about 10–25 $\times$ 10^6 stars down to $V \simeq 14$–15. They will also permit the extraction of individual abundances in 2–5 $\times$ 10^6 stars down to $V \simeq 12$–13.

3.4 Rotational velocities

The analysis of stellar spectra obtained with *Gaia*-RVS will, in addition to other stellar characteristics, enable the determination of the projected rotational velocity ($v \sin i$) of individual stars. The impact of the *Gaia* contribution to stellar rotation astrophysics depends primarily on the precision obtained on $v \sin i$ and on the dependence of this precision on stellar type and magnitude.

The spectroscopic determination of $v \sin i$ is based on the rotational broadening of spectral lines. Analysis methods used to determine $v \sin i$ include fitting by least squares, measurement of FWHM, estimations of the width of the correlation peak, deconvolution and Fourier transforms.

In order to estimate the precision of rotational velocities obtained from *Gaia* spectra, we performed simulations on synthetic Kurucz stellar spectra and used the simple least-squares fit method. The simulations and results presented here are for the RVS spectral resolution $R = 11\,500$ (for results obtained for $R = 5000$–$20\,000$ see Gomboc 2003).

The simulation starts by choosing a stellar type (i.e. a spectrum with given $T_{\rm eff}$, $\log g$, [Fe/H], [α/Fe]) and original $v \sin i$. This spectrum is used to generate RVS-like spectra using the RVS simulator described in Section 3.2. Afterwards, comparisons between simulated and noise-free templates with various $v \sin i$ are performed and the template with the minimum square deviation is taken as the best fit. The precision is taken to be the standard deviation of the

[6] The variation of line intensity responses with the atmospheric parameters is well detailed in table 4 of Cayrel & Jugaku (1963).

[7] The median signal-to-noise ratio per resolution element of the library is 85.

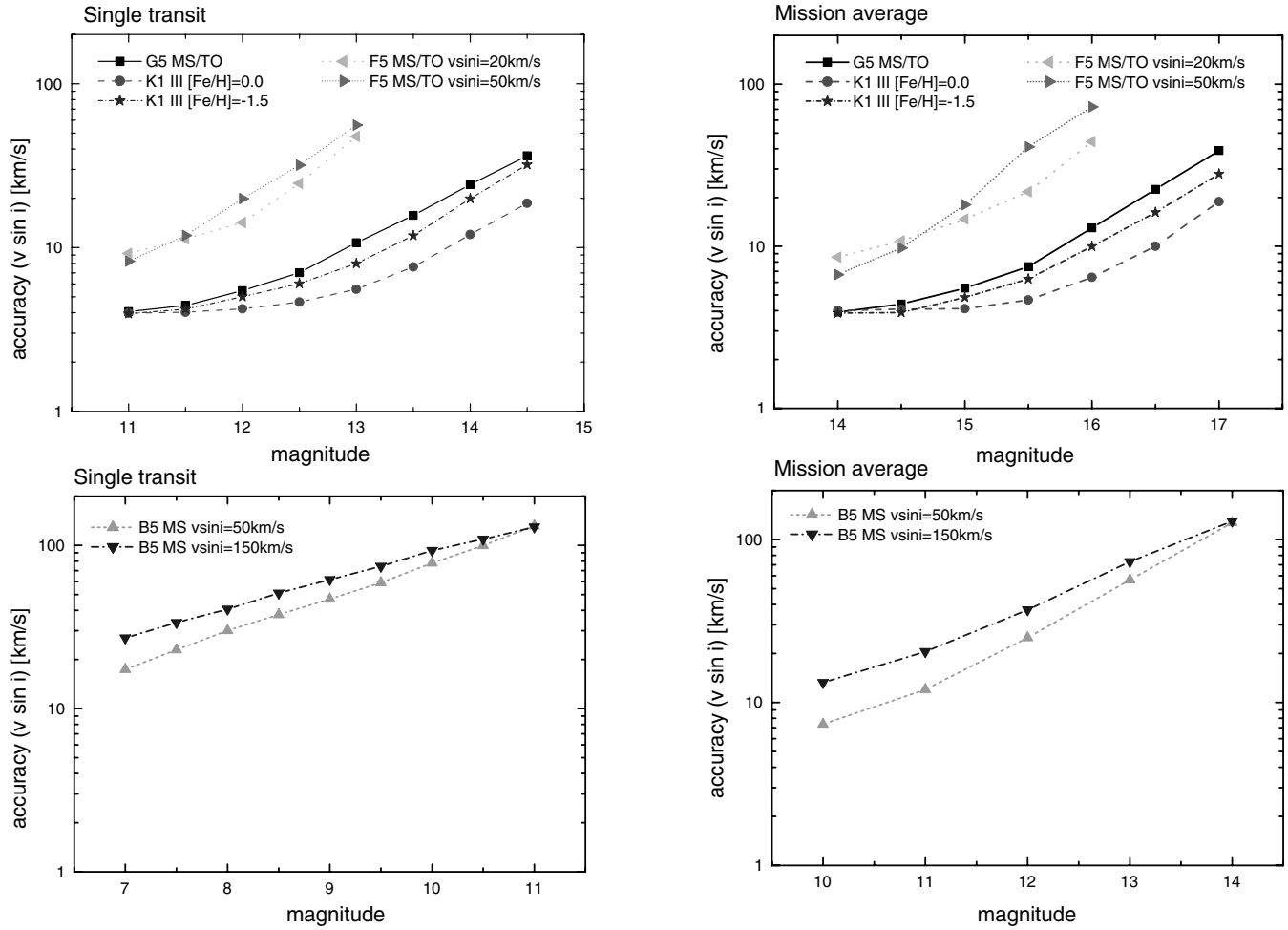

Figure 8. Precision of $v \sin i$ for a single stellar transit over the RVS focal plane (left) and at the end of the mission (right) as a function of magnitude and for the stellar types: K1 III, G5 MS/TO and F5 MS/TO (top) and B5 MS (bottom).

differences between the original and recovered $v \sin i$ (number of trials $N = 1000$).

To estimate the *Gaia*-RVS capabilities, simulations were performed for five out of the six stellar types representative of the different Galactic populations listed in Table 3. The F2 supergiant was not considered in this study, because the macro-turbulent motion in its pulsating atmosphere affects the line profiles, which cannot therefore be used to estimate the rotational velocity.

As the first step towards a detailed and more accurate estimation of the precision of $v \sin i$ determinations, only single-parameter fits were performed. This is the best-case scenario, because it is assumed that the other stellar parameters ($T_{\rm eff}$, $\log g$, [Fe/H], [α/Fe], $V_{\rm r}$) are exactly known and in the fitting procedure spectra that differ only in $v \sin i$ are used. The results are presented in Fig. 8. Precisions of $\sigma_{v \sin i} \simeq 5$ km s^{-1} should be obtained at the end of the mission for $V \simeq 15$ late-type stars. For B5 MS stars, precisions (at the end of the mission) of $\sigma_{v \sin i} \leqslant$ 10–20 km s^{-1} should be obtained up to $V \simeq$ 10–11.

The distributions of estimated $v \sin i$ exhibit a small bias of a few kilometres per second at the 'bright' end, which increases at fainter magnitudes. The errors due to the bias are included in the performances presented in Fig. 8.

In practice, the estimates of $T_{\rm eff}$, $\log g$, [Fe/H], [α/Fe] and $V_{\rm r}$ obtained by *Gaia* will have their own uncertainties, which will influence the precision of the $v \sin i$ determination. To estimate the influence of those uncertainties on the precision of the estimated rotational velocity, similar simulations were performed but the original spectrum was fitted with spectral templates that had one of the parameters ($T_{\rm eff}$, $\log g$, [Fe/H], [α/Fe] or $V_{\rm r}$) offset from its true value. Results are still preliminary, but suggest that an offset of 0.5 in $\log g$ does not substantially influence the precision of the estimated rotational velocity; the precision of $v \sin i$ is not significantly affected by a mismatch of up to 125 K in effective temperature; errors of 0.1 dex in metallicity do not seem to affect significantly the precision of $v \sin i$, while a 0.25-dex mismatch leads to degraded rotational velocities ($\sigma > 10$ km s^{-1}); and errors in radial velocity of 10 km s^{-1} lead to errors in rotational velocities of more than 10 km s^{-1}.

The results presented in Fig. 8 are considered only as a first-order estimation of the performance of *Gaia* in the field of stellar rotation determination. These results were obtained using synthetic stellar spectra and, therefore, modelling uncertainties and chemical composition peculiarities were not taken into account. Furthermore, in regions of high stellar density, the effect of crowding will also undoubtedly degrade the determination of the rotational broadening of spectral lines. The preliminary results also show that the effects of the combined errors in template parameters ($T_{\rm eff}$, $\log g$, [Fe/H], [α/Fe], $V_{\rm r}$) are not easy to predict. While all the results presented here were obtained by single-parameter ($v \sin i$) fitting, more accurate estimations of the performance will be obtained in multi-parameter fitting simulations.

The performance of other analysis techniques will also be assessed in future work. For example, cross-correlation techniques would allow us to disentangle the combined effect of rotational broadening, [Fe/H] and radial velocity, which influence, respectively, the width, the area and the position of the cross-correlation function. Moreover, using a box-shaped template would make the determination less sensitive to spectral mismatch.

3.5 Interstellar reddening

Gaia will accurately place all the observed stars in a three-dimensional representation of the Galaxy. The synergy between spectroscopy and multi-band photometry will allow *Gaia* to quantify the reddening law and the amount of extinction of interstellar origin in any direction and to any distance through the Galaxy. Continuity of the reddening along the line of sight will serve to isolate *deviant* points during the iterative building of the 3D Galactic extinction map. Most of these deviant points will either be due to the use of incorrect models for the intrinsic energy distributions or to circumstellar absorption.

A direct probe, independent of the modelling of the intrinsic energy distribution of the targets, would be valuable in calibrating the zero point and scale of the three-dimensional extinction map during its iterative assembly, in distinguishing between the alternative causes of deviation mentioned above and in providing some clues to the nature of the intervening absorbing material.

Gaia spectroscopy can provide such a direct probe. This is not in the form of atomic absorption lines, however, because no sufficiently strong resonant line lies within the *Gaia* spectroscopic interval. Such atomic absorption lines would trace the gaseous phase of the interstellar/circumstellar medium and a gas-to-dust ratio would have to be adopted in order to convert it into extinction. The interstellar medium, however, also manifests itself on spectra with absorption features other than those of atomic origin. These are termed diffuse interstellar bands (DIBs).

One such DIB lies right at the centre of the *Gaia*-RVS spectral range, at 862.0 nm, where no significant spectral features appear in the spectra of hot stars (cf. Munari & Tomasella 1999) – the best suited to trace interstellar absorption to the furthest distances. Munari (1999) was the first to investigate this band in detail and found a remarkable correlation of its intensity with reddening. Such a relation is unusual among DIBs, which on average show only a mild correlation with reddening (Herbig 1995). Munari (2000) enlarged the sample of investigated stars (covering a larger range of Galactic coordinates and distances) and reinforced the evidence for such a relation, which takes the form (Fig. 9)

$$E(B–V) = 26.9 \times \mathrm{EW\,[nm]}, \quad (2)$$

where EW is the equivalent width of the 862.0-nm DIB. Such a tight relation with reddening suggests a direct association between the carrier(s) of the 862.0-nm DIB and the dust phase of the interstellar medium. The dimensions and composition of interstellar dust grains change through the Galaxy leading to the known effects of the 217.5-nm bump or the ultraviolet slope of the extinction law. It may be expected that these changes will affect the slope of equation (2), which can be generalized to cylindrical coordinates mapping the 3D structure of the Galaxy as

$$E(B–V) = \alpha(l, b, \mathrm{D}) \times \mathrm{EW\,[nm]}. \quad (3)$$

Both the extinction and reddening law map the solid phase of the interstellar medium (i.e. the dimensions and chemistry of the dust grains). The nature of the DIB carriers is still unknown, although

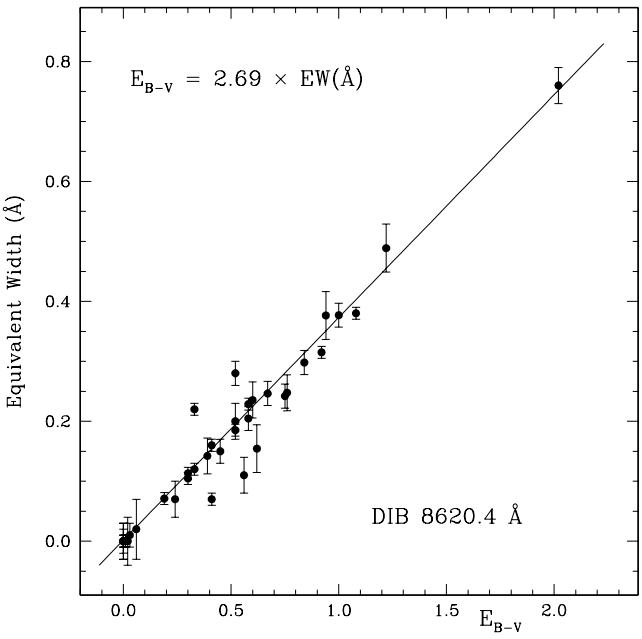

Figure 9. Correlation between the equivalent width of the 862.0-nm DIB and reddening for stars covering a range of Galactic coordinates as observed in Asiago (from Munari 2000).

they are generally believed to be associated with complex molecules, and this makes DIBs potentially useful for tracing (at least in part) the gaseous phase of the interstellar medium. It may be expected that regions deviating from the dust characteristics of the diffuse interstellar medium (as in some circumstellar nebulae and winds) will display a 862-nm DIB deviating from the above relation. In this regard, while *Gaia* photometry will be by far the main tool for the derivation of reddening information, the 862-nm DIB appears to be a useful probe of the conditions within the interstellar medium. For example, HD 62542 has one of the most extreme ultraviolet extinction curves known, featuring a very broad, shortwardly-displaced 217.5-nm bump and an extremely steep far-UV rise. In spite of an estimated $E(B–V) = 0.35$, it does not show appreciable signs of classical 578.0, 579.7, 627.0, 628.4 and 661.4-nm DIBs in its optical spectrum (Snow et al. 2002).

An 862.0-nm DIB as weak as that corresponding to $E(B–V) = 0.10$ should be easily identifiable on the $R = 11\,500$ *Gaia*-RVS spectra of all early-type stars with $\mathrm{S/N} \geqslant 100$. This will provide a great opportunity for the direct probing of the interstellar and circumstellar medium, independent of the photometric approach. Additional, dedicated, ground-based observations for investigating the nature and behaviour of the 862-nm DIB in more detail prior to the *Gaia* launch are to be encouraged.

3.6 Data archiving, calibration and analysis

The development of the on-ground data archiving and processing system is one of the key challenges during the preparation for the RVS and for *Gaia* in general. During the 5-yr mission, *Gaia* will collect about 10–15 billion spectra of $\simeq$100–150 million stars as well as astrometric data and multi-band photometry for about a billion stars. The calibration and analysis of such a huge amount of heterogeneous data (all spectral types and luminosity classes including variable and peculiar stars, single and multiple systems, very-different field stellar densities and therefore levels of

crowding, different temporal sampling as a function of Galactic coordinates, three different instruments), as well as the particular observing mode (continuous and repeated scans of the celestial sphere) require new, robust and fully-automated methods to be developed. The RVS data will not be processed independently of the astrometric and photometric observations: on the contrary, specific methods will be developed to calibrate and analyse the *Gaia* data, as much as possible, in a global way using the whole body of information provided by the three instruments.

The *Gaia* Data base Access and Analysis Study (GDAAS), 2000–2004, is developing a prototype of the data archiving and processing system. At the time of writing, mid-2004, a prototype of the data model and archiving system is in place and several algorithms, including the astrometric global iterative solution, have been implemented and tested (Figueras et al. 2003). By the end of the study, more than 20 algorithms, including a non-optimized derivation of the radial velocities, should be in place. The GDAAS activity will be replaced from ∼2006 by the development of the full *Gaia* archiving and analysis system.

In parallel with the development of data processing tools, studies are in progress to improve our knowledge of atomic and molecular data, to refine the computation of stellar models and synthetic spectra and to build libraries of observed reference spectra. All this information will be used by the calibration and analysis processes and their quality will be directly reflected in the accuracy of the derived stellar and interstellar parameters.

4 CONCLUSIONS

The RVS is a $2^\circ \times 1\overset{\circ}{.}61$ integral field spectrograph observing in TDI scan mode over the wavelength range [848, 874] nm with a resolving power $R = \lambda/\Delta\lambda = 11\,500$. The RVS will provide a rich harvest of stellar and interstellar parameters: radial velocities up to magnitude $V \simeq 17$–18, rotational velocities with precisions for late-type stars of $\sigma_{v \sin i} \simeq 5$ km s^{-1} at $V \simeq 15$, individual element abundances (for stars with $V \leqslant 12$–13 mag) and interstellar reddening. It will also contribute, together with the astrometric and photometric data, to the determination of the atmospheric parameters of stars brighter than $V \simeq 14$–15. Moreover, many stellar processes will imprint their distinctive signatures in the RVS spectra: e.g. pulsation and variability, mixing, accretion, winds and mass loss. Finally, the large number of epochs of observation will make it possible to detect and characterize binary and multiple stellar systems as well as periodic and transient phenomena.

During the two years 2001–2002, the RVS preparation studies were mainly focused on the definition of the instrument scientific case and on the comparison of the performance of the different possible configurations. These studies converged in late 2002 with the selection of the baseline concept. Work on RVS is now mainly devoted to:

(i) the optimization and development of the instrument design;

(ii) the simulation of more realistic RVS-like spectra that will be used to refine the evaluation of the performance of the spectrograph; and

(iii) the definition and development of the on-board and on-ground data processing algorithms.

ACKNOWLEDGMENTS

We would like to thank the ESA and industry teams preparing the *Gaia* mission for their active and efficient support. We are very grateful to R. Kurucz, F. Kupka, N. Piskunov and the VALD people for making their software packages and molecular data available to the community. DK, FT, FA, CT and SM acknowledge financial support from CNES. MIW acknowledges financial support from PPARC. TZ, AG, AP and UJ acknowledge the financial support of the Slovenian Ministry of Education, Science and Sport. AG also acknowledges the receipt of Marie Curie Fellowship from the European Commission. We are grateful to our referee, G. Gilmore, for useful comments that improved the quality of the manuscript.

REFERENCES

Allende Prieto C., 2003, MNRAS, 339, 1111
Andrillat Y., Jaschek C., Jaschek M., 1995, A&AS, 112, 475
Bailer-Jones C. A. L., 2000, A&A, 357, 197
Bailer-Jones C. A. L., 2002, Ap&SS, 280, 21
Bailer-Jones C. A. L., 2003, in Munari U., ed., ASP Conf. Ser. 298, *Gaia* Spectroscopy, Science and Technology. Astron. Soc. Pac., Monte-Rosa, CA, p. 199
Binney J. J., Dehnen W., Houk N., Murray C. A., Penston M. J., 1997, in ESA, ed., ESA SP-402: Hipparcos – Venice '97. ESA, Venice, p. 473
Carquillat M. J., Jaschek C., Jaschek M., Ginestet N., 1997, A&AS, 123, 5
Cayrel R., 1988, in Cayrel de Strobel G., Spite M., eds, Proc. IAU Symp. 132, The Impact of Very High S/N Spectroscopy on Stellar Physics. Kluwer Academic, Paris, p. 345
Cayrel R., Jugaku J., 1963, Annales d'Astrophysique, 26, 495
Cayrel R., Perrin M.-N., Barbuy B., Buser R., 1991, A&A, 247, 108
Cenarro A. J., Cardiel N., Gorgas J., Peletier R. F., Vazdekis A., Prada F., 2001, MNRAS, 326, 959
Chen B., 1997, ApJ, 491, 181
David M., 2001, RVS-MD-001, ESA report
David M., 2002a, RVS-MD-002, ESA report
David M., 2002b, RVS-MD-003, ESA report
Desidera S., Munari U., 2003, in Munari U., ed., ASP Conf. Ser. 298, *Gaia* Spectroscopy, Science and Technology. Astron. Soc. Pac., Monte-Rosa, CA, p. 85
ESA, 2000, *Gaia*: Composition, Formation and Evolution of the Galaxy. ESA, Technical report ESA-SCI(2000)4
Favata F., Perryman M., 1995, ESA SP, 379, 153
Figueras F., Torra J., Serraler I., Masana E., Luri X., Jordi C., Llimona P., Pérez P., 2003, UB-GDAAS-TN-020, ESA report
Fluks M. A., Plez B., The P. S., de Winter D., Westerlund B. E., Steenman H. C., 1994, A&AS, 105, 311
Gerbaldi M., Gómez A., Grenier S., Turon C., Faraggiana R., 1989, Messenger, 56, 12
Gomboc A., 2003, in Munari U., ed., ASP Conf. Ser. 298, *Gaia* Spectroscopy, Science and Technology. Astron. Soc. Pac., Monte-Rosa, CA, p. 285
Herbig G. H., 1995, ARA&A, 33, 19
Howell S. B., Everett M. E., Tonry J. L., Pickles A., Dain C., 2003, PASP, 115, 1340
Katz D., 2000, PhD thesis, Univ. Paris VII
Katz D., Soubiran C., Cayrel R., Adda M., Cautain R., 1998, A&A, 338, 151
Katz D., Viala Y., Gomez A., Morin D., 2002, in Bienaymé O., Turon C., eds, EAS Pub. Ser. Vol. 2, *Gaia*: A European Space Project. EDP Sciences, Les Houches, p. 63
Kupka F., Piskunov N., Ryabchikova T. A., Stempels H. C., Weiss W. W., 1999, A&AS, 138, 119
Kurucz R., 1993a, ATLAS9 Stellar Atmosphere Programs and 2 km/s grid. Smithsonian Astrophysical Observatory, Cambridge, MA, CD-ROM No. 13
Kurucz R., 1993b, SYNTHE Spectrum Synthesis Programs and Line Data. Smithsonian Astrophysical Observatory, Cambridge, MA, CD-ROM No. 18
Lindegren L., 1998, SAG-LL-014, ESA report
Lindegren L., 2000, SAG-LL-030, ESA report
Lindegren L., 2001, SAG-LL-035, ESA report

Marrese P. M., Boschi F., Munari U., 2003, A&A, 406, 995
Mayor M. et al., 1989, Messenger, 56, 12
Mignard F., 2002, A&A, 393, 727
Montes D., Martin E. L., 1998, A&AS, 128, 485
Montes D., Ramsey L. W., Welty A. D., 1999, ApJS, 123, 283
Munari U., 1999, Baltic Astronomy, 8, 73
Munari U., 2000, in Porceddu I., Aiello S., eds, Proc. Ita. Phys. Soc. Conf. Vol. 67, Molecules in Space and in the Laboratory. Carloforte, p. 179 (also astro-ph/0010271)
Munari U., 2003, in Munari U., ed., ASP Conf. Ser. 298, *Gaia* Spectroscopy, Science and Technology. Astron. Soc. Pac., Monte-Rosa, CA, p. 227
Munari U., Tomasella L., 1999, A&AS, 137, 521
Munari U., Agnolin P., Tomasella L., 2001, Baltic Astronomy, 10, 613
Munari U., Zwitter T., Katz D., Cropper M., 2003, in Munari U., ed., ASP Conf. Ser. 298, *Gaia* Spectroscopy, Science and Technology. Astron. Soc. Pac., Monte-Rosa, CA, p. 275
Pavlenko Y. V., Marrese P. M., Munari U., 2003, in Munari U., ed., ASP Conf. Ser. 298, *Gaia* Spectroscopy, Science and Technology. Astron. Soc. Pac., Monte-Rosa, CA, p. 451
Pernechele C., Munari U., 2003, in Munari U., ed., ASP Conf. Ser. 298, *Gaia* Spectroscopy, Science and Technology. Astron. Soc. Pac., Monte-Rosa, CA, p. 93
Perryman M. A. C., 1995, in Høg E., Kenneth P., eds, Proc. IAU Symp. 166, Astronomical and Astrophysical Objectives of Sub-Milliarcsecond Optical Astrometry. Kluwer Academic, The Hague, p. 211
Perryman M. A. C. et al., 2001, A&A, 369, 339
Piskunov N. E., 1992, in Glagolevskij Y. V., Romanyuk I. I., eds, Stellar Magnetism. Nizhnij Arkhyz, p. 92
Piskunov N. E., Kupka F., Ryabchikova T. A., Weiss W. W., Jeffery C. S., 1995, A&AS, 112, 525
Pourbaix D., Jancart S., 2003, in Munari U., ed., ASP Conf. Ser. 298, *Gaia* Spectroscopy, Science and Technology. Astron. Soc. Pac., Monte-Rosa, CA, p. 345
Reininger F. M., 1994, in Cerutti-Maori M. G., Roussel P., eds, Proc. SPIE Vol. 2209, Space Optics 1994: Earth Observation and Astronomy, p. 332
Ryabchikova T., Piskunov N., Stempels H., Kupka F., Weiss W., 1999, Proc. 6th International Colloquium on Atomic Spectra and Oscillator Strengths. Victoria BC, Physica Scripta, Vol. 83, p. 162
Serote Roos M., Boisson C., Joly M., 1996, A&AS, 117, 93
Snow T. P., Welty D. E., Thorburn J., Hobbs L. M., McCall B. J., Sonnentrucker P., York D. G., 2002, ApJ, 573, 670
Sordo R., Munari U., 2003, in Munari U., ed., ASP Conf. Ser. 298, *Gaia* Spectroscopy, Science and Technology. Astron. Soc. Pac., Monte-Rosa, CA, p. 221
Soubiran C., 2001, RVS-CS-001, ESA report
Thevenin F., Foy R., 1983, A&A, 122, 261
Thevenin F., Jasniewicz G., 1992, A&A, 266, 85
Thevenin F., Bijaoui A., Katz D., 2003, in Munari U., ed., ASP Conf. Ser. 298, *Gaia* Spectroscopy, Science and Technology. Astron. Soc. Pac., Monte-Rosa, CA, p. 291
Torra J., Chen B., Figueras F., Jordi C., Luri X., 1999, Baltic Astronomy, 8, 171
Valdes F., Gupta R., Rose J. A., Singh H. P., Bell D. J., 2004, ApJS, 152, 251
Wilkinson M. I. et al. 2004, MNRAS, submitted
Zwitter T., 2002, A&A, 386, 748
Zwitter T., 2003, in Munari U., ed., ASP Conf. Ser. 298, *Gaia* Spectroscopy, Science and Technology. Astron. Soc. Pac., Monte-Rosa, CA, p. 493
Zwitter T., Castelli F., Munari U., 2003, in Munari U., ed., ASP Conf. Ser. 298, *Gaia* Spectroscopy, Science and Technology. Astron. Soc. Pac., Monte-Rosa, CA, p. 215
Zwitter T., Castelli F., Munari U., 2004, A&A, 417, 1055

This paper has been typeset from a TEX/LATEX file prepared by the author.